JOURNAL OF PROPULSION AND POWER
Vol. 12, No. 2, March–April 1996

Flutter Analysis of Propfans Using a Three-Dimensional Euler Solver

R. Srivastava* and T. S. R. Reddy*
University of Toledo, Toledo, Ohio 43606
and
O. Mehmed†
NASA Lewis Research Center, Cleveland, Ohio 44135

A three-dimensional aeroelastic solver is developed and applied to investigate the flutter of a propfan. The unsteady airloads are obtained by solving three-dimensional Euler equations. An implicit–explicit hybrid scheme is used to reduce computational time for the solution of Euler equations. A finite element model is used to obtain structural properties, and a deforming grid technique is used to simulate elastic deformations of the blade. The aeroelastic equations are formulated in normal mode form and are solved for flutter using both the time and frequency domain methods. The analysis is used to calculate the dynamic aeroelastic stability of a single-rotation propfan model for which classical flutter was measured at subsonic relative flows. Comparisons with the experimental data and other calculated results are given.

Introduction

PROPFANS are capable of extending the high efficiency of propellers to high cruise Mach numbers.[1] However, the special features of propfans can lead to classical flutter. Propfan flutter has been investigated in wind-tunnel tests of some single rotation models.[2,3]

Several analytical methods have been developed to calculate flutter in Refs. 2, 4, and 5. The unsteady aerodynamic loads are calculated using a two-dimensional unsteady linear cascade theory with a correction for blade sweep. Structural models ranging from typical section to swept beams to finite elements have been used in these analyses. A linear three-dimensional steady and unsteady aerodynamic theory for advanced turboprops with subsonic leading edge was presented in Ref. 6. An aeroelastic code (ASTROP3) based on this theory has been applied to analyze a composite propfan model (SR3C-X2) in subsonic flow in Ref. 7. The equations were formulated in terms of normal modes, the normal modes being obtained from a finite element analysis. Good correlation of flutter speeds between theory and experimental data was reported in Ref. 7 for the SR3C-X2 propfan. The correlation, however, was not good using ASTROP3 to calculate flutter for the SR5 propfan.[8] For this case, the tip relative Mach numbers ranged from 1.0 to 1.1 with transonic flow on the blades. It was stated in Ref. 8 that the flow nonlinearities in transonic flow combined with a mean angle of attack and high blade sweep may be the reasons for the poor correlation.

Flutter analysis methods using computational fluid dynamics (CFD) have now been developed at NASA Lewis and can be used to better analyze propellers with blades having high sweep and operating in transonic flow. Aeroelastic formulations for the two-dimensional cascades using the linearized potential equation,[9] full potential equation,[10] and Euler and Navier–Stokes equations[11] have been developed. A three-dimensional aeroelastic code based on the full potential aerodynamic equation and a finite element structural model has been reported.[12,13] Two propfans, SR3C-X2 and F21, were analyzed[12,13] for flutter. The analysis was not able to predict the measured flutter of F21. The presence of a leading-edge vortex is mentioned as a possible cause for this discrepancy in Ref. 12.

The numerical analysis methods developed previously, for the aeroelastic analysis of propfans, are based on either linear aerodynamic analysis or irrotational flow assumptions. These methods do not provide accurate unsteady airloads in flowfields with strong rotational flow arising because of the presence of shock and its motion. Euler equation models are able to capture the physics involved in modeling the nonlinearities arising because of the presence of shock and its motion, and will provide a more accurate aeroelastic analysis. Towards this objective a three-dimensional aeroelastic code based on Euler equations is developed and reported in this article. The unsteady Euler equations are solved using an implicit–explicit hybrid scheme.[14] The hybrid numerical scheme for the aerodynamic solution has been validated for several flight conditions and different propfan configurations in Ref. 14. It has also been successfully applied to calculate the static aeroelastic stability of a single rotation propfan in Ref. 15.

The aeroelastic equations are formulated in normal modes obtained from a finite element analysis. The governing aeroelastic equations are solved in both the time and frequency domains to calculate flutter. Arbitrary number of modes can be included in the analysis and all interblade phase angles of interest are solved for flutter.

The primary objective of the present work is to develop and apply the aeroelastic analysis method. The results presented are limited to flutter conditions of the SR3C-X2 propfan. All of the SR3C-X2 flutter conditions are at subsonic relative tip Mach numbers and provide good test cases for initial code verification. Comparison with other numerical calculations for the SR3C-X2 flutter conditions is also made. Future work will include the calculation of propfan flutter at transonic tip relative flow velocities.

Formulation

The formulation of the aerodynamic analysis is described only briefly here, followed by a detailed description of the aeroelastic analysis. A detailed description of the aerodynamic analysis is available in Ref. 14.

Received May 12, 1994; revision received July 18, 1995; accepted for publication Nov. 8, 1995.

*Senior Research Associate; currently Resident Research Associate, NASA Lewis Research Center, Cleveland, OH 44135. Member AIAA.

†Senior Research Engineer; currently Resident Research Associate, NASA Lewis Research Center, Cleveland, OH 44135. Member AIAA.

Aerodynamic Analysis

The unsteady Euler equations, in conservation form, cast in a body-fitted generalized coordinate system are solved using a hybrid algorithm. The flux terms in two directions (streamwise and azimuthal) are treated implicitly, whereas the radial direction flux terms are treated semi-implicitly. The first-order-accurate Euler rule is used for time differencing, and second-order-accurate central difference is used for spatial derivatives. Second/fourth-difference explicit dissipation and a second-order implicit dissipation are used to make the scheme stable and to reduce high-frequency errors. The flux terms being treated implicitly are linearized, as in the Beam–Warming algorithm,[16] about their values at the previous time level, resulting in a block pentadiagonal system of equations for the changes in the flow properties. The pentadiagonal system is approximately factored into two block tridiagonal system of equations, and solved using the Thomas algorithm. This method requires only two inversions of the block tridiagonal matrix, in the two implicit directions, as opposed to three for fully implicit schemes. It also reduces the memory requirement almost in half, as only two time levels of information need to be stored at any given time, one of which needs to be only two dimensional.

The flowfield around the multiblade propfan is solved using a multiblock grid technique. The flow variables at the boundaries are updated explicitly after the governing equations have been solved for the interior flowfield. On the solid surfaces of blade and nacelle the no-penetration condition is applied to the velocity component normal to the solid surface. The velocity components tangential to the solid surface, the pressure and the density, are extrapolated from the interior of the domain. At the inflow and outflow boundaries, depending upon the flow Mach number, the characteristic quantities are either extrapolated or fixed. For the subsonic outflow boundary the static pressure is obtained by solving the radial equilibrium equation.[17]

The block interface fluid boundaries are updated depending upon the flowfield being analyzed. For axisymmetric inflow and zero interblade phase flutter, only one blade passage is solved, enforcing periodicity at the fluid block interface boundaries. For asymmetric inflow or for nonzero interblade phase flutter, all blade passages are solved. In this case, the boundaries are updated by enforcing the second derivative of the flow variables to be zero, at the boundary from the nodes across the boundary of the adjoining blocks.

Aeroelastic Analysis

In the present analysis the hub is assumed to be rigid. This assumption simplifies the problem by structurally decoupling the blades from one another. Consequently, each blade can be modeled separately. Even though the blades are structurally decoupled, they are aerodynamically coupled. The large sweep and twist of propfan blades couple the blade bending and torsional motions. This requires using a finite element structural model that accounts for centrifugal effects on blade stiffness. The governing nonlinear aeroelastic equations for each blade, with viscous proportional damping, can be written as follows:

$$[M]\{\ddot{u}\} + [C]\{\dot{u}\} + [[K_s] + [K(u)]]\{u\} = \{P(\{u, \dot{u}\}, t)\} \quad (1)$$

where $\{u\}$ is the vector of blade deflections, $[M]$ is the mass matrix, $[C]$ is damping matrix, $[K_s]$ is the centrifugal softening matrix, $[K(u)]$ is the nonlinear stiffness matrix that is a function of $\{u\}$, $P(\{u, \dot{u}\})$ is the equivalent aerodynamic force vector, and $(\dot{})$ represents the time derivative. Equation (1) is nonlinear and can be solved by directly integrating in time. However, this requires an iterative method at every time step to obtain a converged solution for displacements and forces, making it computationally expensive. If one is interested only in flutter inception, the dynamic behavior of the propfan may be assumed to be linear in the vicinity of a nonlinearly reached steady state. The nonlinear aeroelastic equation [Eq. (1)] can be written for perturbed quantities and solved using a normal mode analysis technique. Defining

$$\{u\} = \{u_0\} + \{\Delta u(t)\}$$

$$\{P(\{u\}, t)\} = \{P(\{u_0\})\} + \{\Delta P(\{\Delta u\}, t)\}$$

where $\{u_0\}$ and $\{P(\{u_0\})\}$ are the steady-state values, and $\{\Delta u(t)\}$ and $\{\Delta P(\{\Delta u\}, t)\}$ are perturbations from $\{u_0\}$ and $\{P(\{u_0\})\}$, respectively. The general vibratory motion of the blade, about a steady-state mean, can be expressed as a superposition of the contributions of the various normal modes:

$$\{\Delta u(t)\} = [\phi]^T\{q\} \quad (2)$$

where $\{q\}$ is the generalized displacement vector and $[\phi]$ is the modal matrix. The aeroelastic equations in perturbed quantities can then be written in normal modes as

$$[M_g]\{\ddot{q}\} + [C_g]\{\dot{q}\} + [K_g]\{q\} = \{F\} \quad (3)$$

where

$$[M_g] = [\phi]^T[M][\phi]$$

$$[C_g] = 2.0\{\zeta\}[M_g]\{\omega\}$$

$$[K_g] = [M_g]\{\omega^2\}$$

$$\{F\} = [\phi]^T\{\Delta P\}$$

$\{\omega\}$ is the natural (in vacuum) frequency, $\{\zeta\}$ is the critical damping ratio, and $\{\Delta P\}$ is the aerodynamic load vector defined as

$$\Delta P_i = (p_u - p_l)_i A r_i \quad (4)$$

where p_u and p_l are the upper and lower surface pressures, respectively, and Ar_i is the area associated with node i. The quantities $[M]$, $\{\omega\}$, and $[\phi]$ are obtained using the finite element analysis. The size of the matrices in Eq. (3) depends on the number of modes included in the analysis. The normal mode aeroelastic equation [Eq. (3)] can be solved using either time domain or frequency domain analysis.

Time Domain Aeroelastic Analysis

The dynamic stability characteristics in the time domain are obtained by perturbing the propfan from the steady state. One of the propfan blades is provided an initial velocity ($\dot{q}_i$, $i = 1, n$) in all of the n normal modes included in the analysis. The response of all the blades to the initial disturbance is calculated by integrating the unsteady Euler equations and the aeroelastic equations [Eq. (3)] sequentially in time to obtain $\{q\}$. The nodal displacements are then obtained using Eq. (2). These displacements are added to the steady-state blade geometry to define the new instantaneous deformed blade shape. Once the new deformed blade shape has been defined, the mesh is updated by linear interpolation. The aerodynamic equations are then solved again to obtain the new loads on the blades. Loads are obtained on all of the blades before the blade deformation calculation is repeated to obtain $\{q\}$ at the next time level. A diverging response of $\{q\}$ is assumed to indicate dynamic instability. For time domain analysis, unlike frequency domain analysis, no a priori information on either the interblade phase angle or the frequency of instability is needed. It is an output of the solution.

Frequency Domain Aeroelastic Analysis

Assuming a linear variation of aerodynamic forces with blade motion, the force $\{F\}$ in Eq. (3) can be written as

$$\{F\} = [A]\{q\} \quad (5)$$

with

$$A_{ij} = \{\phi_i\}^T\{\Delta P\}_j \tag{6}$$

where $\{\Delta P\}_j$, defined by Eq. (4), is the force induced by vibration in mode j, and $\{\phi_i\}$ is the ith mode shape. Hence, A_{ij} is the aerodynamic coefficient for the ith mode because of the motion in the jth mode. The aerodynamic coefficients are obtained using the pulse response method, as a single calculation provides the coefficients for all frequencies of interest. In the pulse response method, the blades are oscillated with a prescribed pulse in a given mode of motion and the aerodynamic transients are calculated. The harmonic response for any required frequency of oscillation is obtained by taking the ratio of the Fourier transform of the aerodynamic transients and the input motion. The pulse must include significant spectral content for the frequencies of interest. For multiple blade analysis, only one blade (reference blade) is moved in any given mode j. The pulse suggested in Ref. 12 is used in the present analysis. The time history of A_{ij} is recorded for all of the blades because of the pulse oscillation of the reference blade in the jth mode. As the analysis requires that the blade be moved in only one normal mode at a time, this procedure is repeated for all of the normal modes of interest.

The stability of the blades is determined using the Laplace transform method described in Ref. 6. Taking the Laplace transform of Eq. (3), the stability can be determined by finding the roots of the equation,

$$\det[M_g s^2 + C_g s + K_g - Q(\sigma, s)] = 0 \tag{7}$$

where σ is the interblade phase angle, and $Q(\sigma, s)$ is obtained by taking the Laplace transform of $[A]$ for each blade and combining them using linear superposition based on the influence coefficient method,[13] for the interblade phase angles of interest. If the real part of any of the roots of Eq. (7) is greater than zero (negative aerodynamic damping), the propeller is unstable for that interblade phase angle. For an N-bladed propfan, there are only N possible interblade phase angles ($\sigma = 2\pi n/N$, $n = 0 \ldots N - 1$) for flutter.[18] Therefore, Eq. (7) is solved for only these possible phase angles. The aeroelastic stability is obtained by solving Eq. (7) as postprocessing after the time history of $[A]$, because of the pulse oscillation, has been recorded. The time histories are recorded until the transients in the aerodynamic coefficients, because of the pulse motion, have died out.

Results and Discussion

The analysis is applied here to predict flutter of the SR3C-X2 propfan. This propfan fluttered with several different blade counts.[3] The analysis is carried out at two measured flutter conditions for four and eight blades operating at advance ratio $J = 3.55$ and blade setting angle β of 61.2 deg. For four blades the flutter was measured at a freestream Mach number $M_\infty = 0.62$, flutter frequency $\omega = 274$ Hz, and interblade phase angle $\sigma = 180$ deg (Ref. 3). For eight blades the flutter was measured at $M_\infty = 0.6$, $\omega = 264$ Hz, and $\sigma = 225$ deg (Ref. 3). It was also stated in Ref. 3 that the flutter occurs in a coupled mode with coupling between the first and second natural modes. For both the four and eight blades, the aeroelastic stability is calculated for $M_\infty = 0.5$ and 0.7, $J = 3.55$, and $\beta = 61.2$ deg. For the four-blade case, the analysis is also carried out at $M_\infty = 0.62$, the Mach number at which flutter was observed. For both configurations, the calculations show that the propfan is stable for the 0.5 Mach condition and unstable for the 0.7 Mach condition. The five cases are investigated using both time and frequency domain analyses.

A typical body fitted H–O grid used for these calculations is shown in Fig. 1. The domain of the calculation at each time step was taken to be the region between two blades with the upper surface of one blade and the lower surface of the adjoining blade as the boundaries of the domain. This region is referred to as blade passage. In general, to model the influence of adjacent blades (cascade effect), the entire propfan with all of the blades (passages) are solved. For each passage there are 100 grid points in the streamwise direction, 33 in the radial direction, and 21 in the azimuthal direction.

In the present work the aeroelastic analysis assumes that all of the blades have identical structural properties (tuned rotor). Hence, it is sufficient to structurally model any one blade. The analysis is carried out by including the first three normal modes and zero structural damping. The blade natural frequencies, mode shapes, and generalized mass and stiffness matrices required for the analysis are obtained from an MSC/Nastran finite element analysis. The finite element model was calibrated by matching the first mode calculated frequency to that of the bench measured first mode blade frequency. The frequencies for the other two modes used in the analysis were higher for the Nastran blade model than measured. For this blade, the first mode is primarily flexural, but also has a large degree of torsion, the second mode is primarily torsional near the tip, and the third mode is primarily second flex.[3]

Four Blades

The time domain results are presented first. The response of the blades because of an initial perturbation, namely the displacement amplitude of the three coupled modes, q_1, q_2, and q_3, for the four blades are plotted in Figs. 2–4. In Fig. 2, the response for $M_\infty = 0.5$ is plotted. The initial perturbation of blade 1 dies out rapidly with negligible motion of the other blades, indicating a stable propfan. Whereas, in Fig. 3 for $M_\infty = 0.7$, the response grows for all of the modes. Even though the perturbation was provided to only one blade, all of the blades become excited and responded with increasing amplitude of the oscillation cycle. Once the responses start increasing, in all of the blades and all of the modes, the frequency of all the modes changes. In each mode, the oscillations start off with respective normal

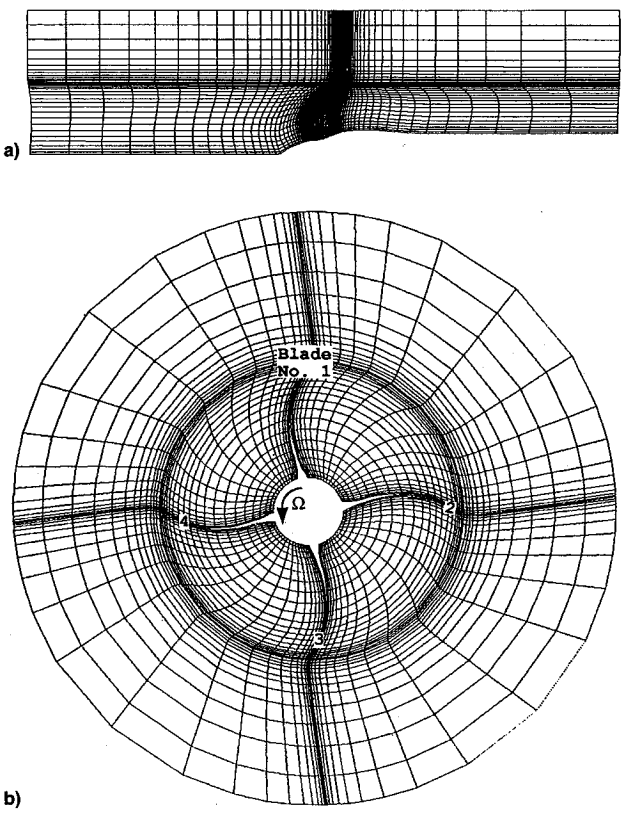

Fig. 1 Typical grid around the blade row. Grid in the a) streamwise and b) azimuthal planes.

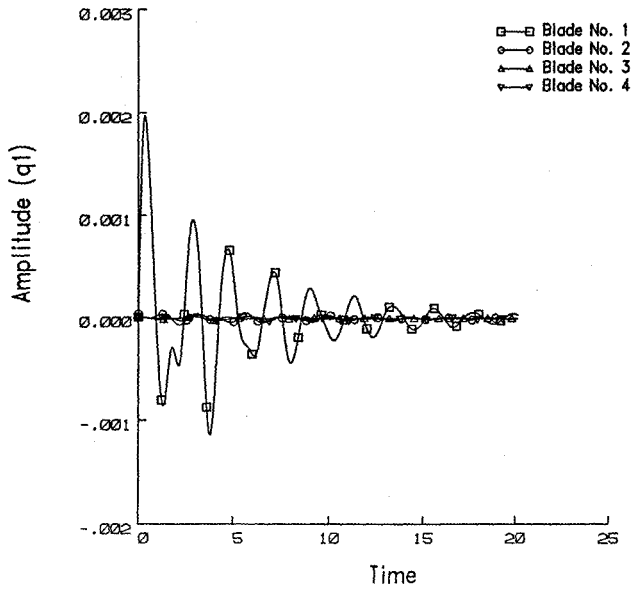

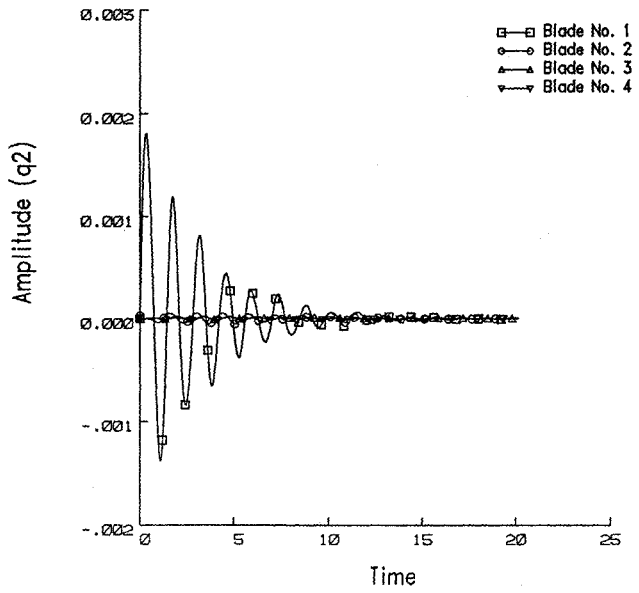

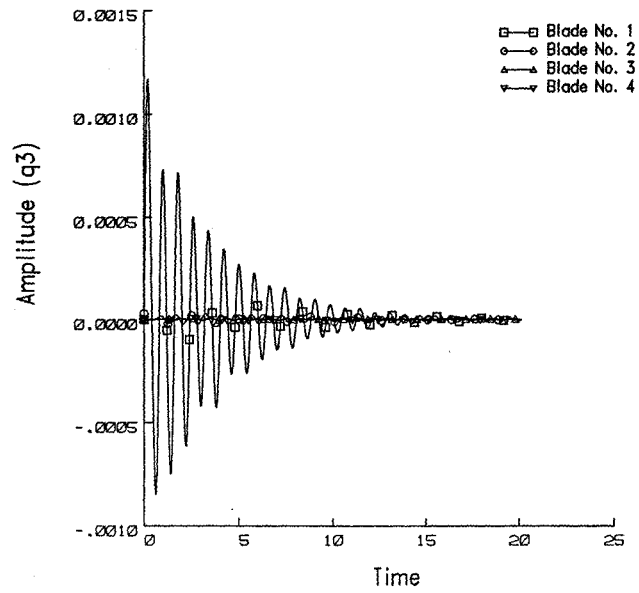

Fig. 2 Response of normal modes for SR3C-X2 with four blades operating at $M_\infty = 0.5$, $J = 3.55$, and $\beta = 61.2$ deg.

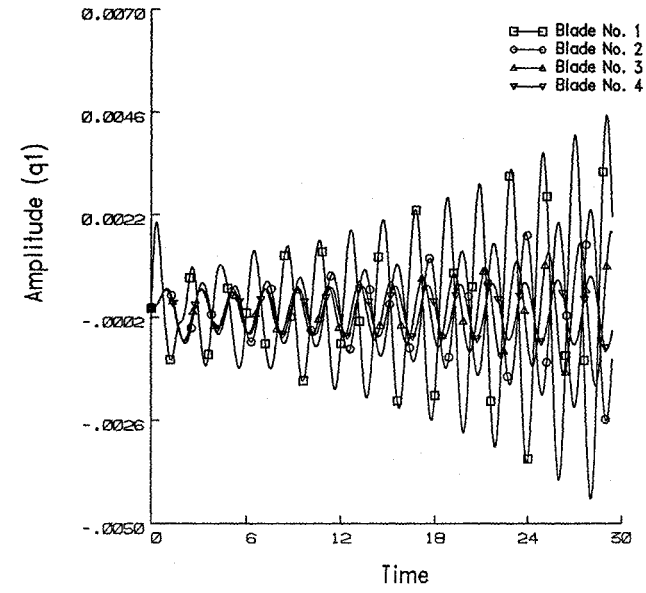

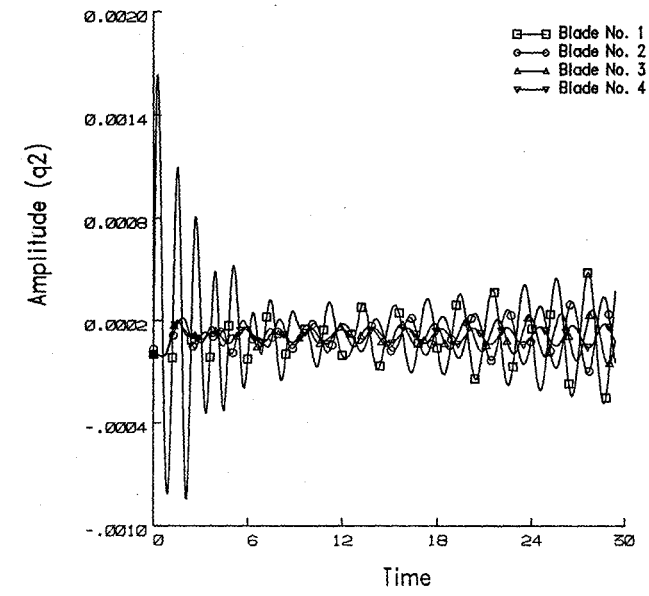

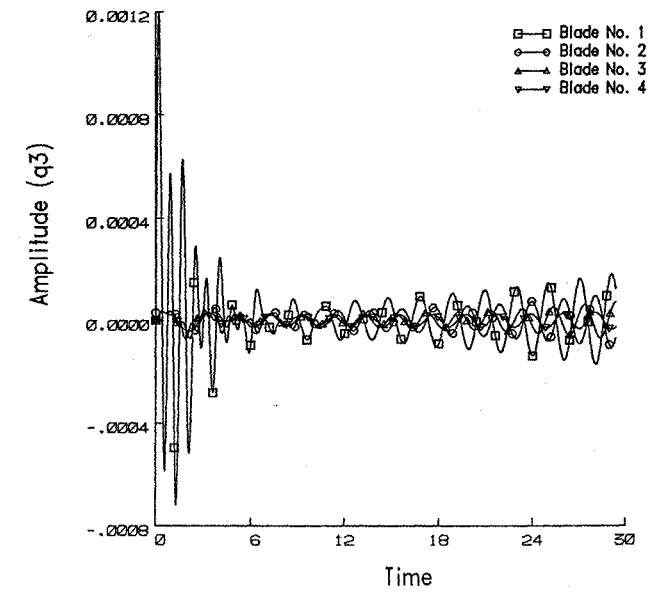

Fig. 3 Response of normal modes for SR3C-X2 with four blades operating at $M_\infty = 0.7$, $J = 3.55$, and $\beta = 61.2$ deg.

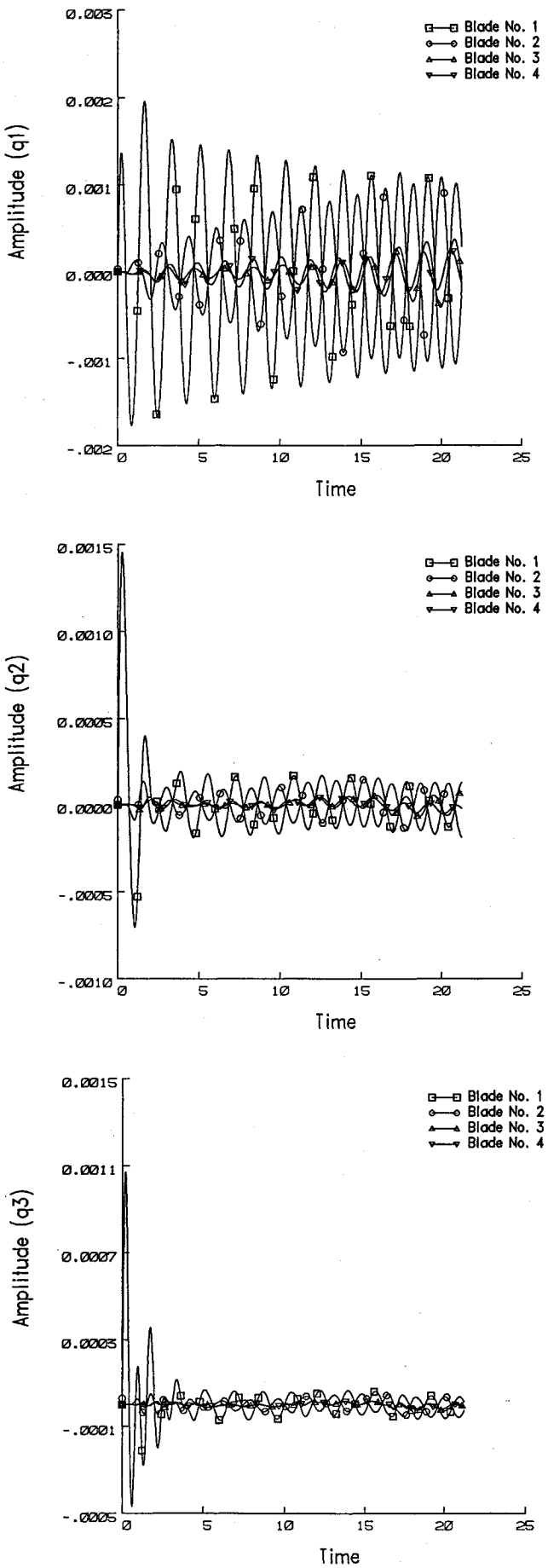

Fig. 4 Response of normal modes for SR3C-X2 with four blades operating at $M_\infty = 0.62$, $J = 3.55$, and $\beta = 61.2$ deg.

mode frequencies, but as the response amplitude starts to increase, the oscillation frequency becomes similar for all of the modes, indicating a flutter response. Observing the last few oscillation cycles on a larger scale plot of Fig. 3, it was seen that the response of blades 1 and 2 are almost out of phase. The same is true for blades 2 and 3, 3 and 4, and 4 and 1. This implies that the interblade phase for flutter is close to 180 deg. These time histories can be Fourier analyzed to obtain the flutter frequency and interblade phase angle. However, for accurate information the aeroelastic analysis needs to be carried out for a significantly larger number of oscillations. At this stage the response frequency and interblade phase-angle calculations are dependent on the length of signal included in the Fourier analysis. As these calculations are expensive, they were run for only such time as to conclusively indicate the stability characteristics of the propfan. The results for $M_\infty = 0.62$ are shown in Fig. 4. The plots of modes two and three show that the response of all the blades are very close to being neutral, as opposed to the other two Mach number cases. For the first mode plot, the response of the perturbed blade and that of the other blades also tend towards a limit cycle response. This indicates that the analysis condition is close to the flutter point. The experimentally measured flutter boundary for this case is at $M_\infty = 0.62$.

The same operating conditions are next used in frequency domain calculations. Since three normal modes are used in the analysis, the calculations are repeated three times, once for each mode, to obtain the unsteady aerodynamic coefficients. The variation of frequency (imaginary part of eigenvalue) with damping (real part of eigenvalue) for all of the possible interblade phase angles ($\sigma = 0$, 90, 180, and 270 deg) for the three Mach number cases, $M_\infty = 0.5$, 0.62, and 0.7 is plotted in Fig. 5. As can be seen, the propfan is stable (real part of eigenvalue is negative) for $M_\infty = 0.5$ and unstable for $M_\infty = 0.7$ (real part of eigenvalue is positive). For $M_\infty = 0.62$, the real part of eigenvalues are very close to zero, with 180- and 270-deg interblade phase angles being marginally unstable and 0 and 90 deg being stable, indicating this condition to be close to flutter boundary. For $M_\infty = 0.62$ and 0.7, the calculations show that the 180-deg phase has the largest positive value of the real part of eigenvalue, implying the 180-deg phase angle mode to be the flutter mode.

Calculated flutter Mach number and interblade phase angle, from both the time and frequency domain analyses, agree well with the measured values. The correlation of calculated flutter frequency, however, is fair. The flutter frequency measured in

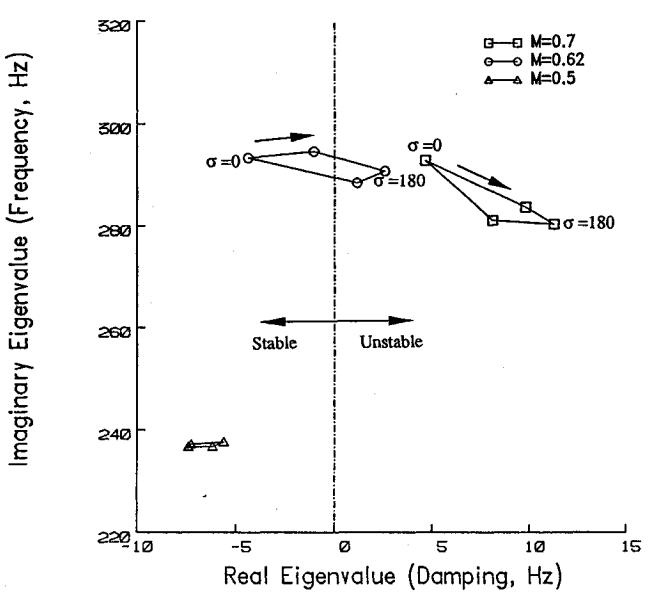

Fig. 5 Eigenvalue plot for SR3C-X2 with four blades operating at $J = 3.55$ and $\beta = 61.2$ deg.

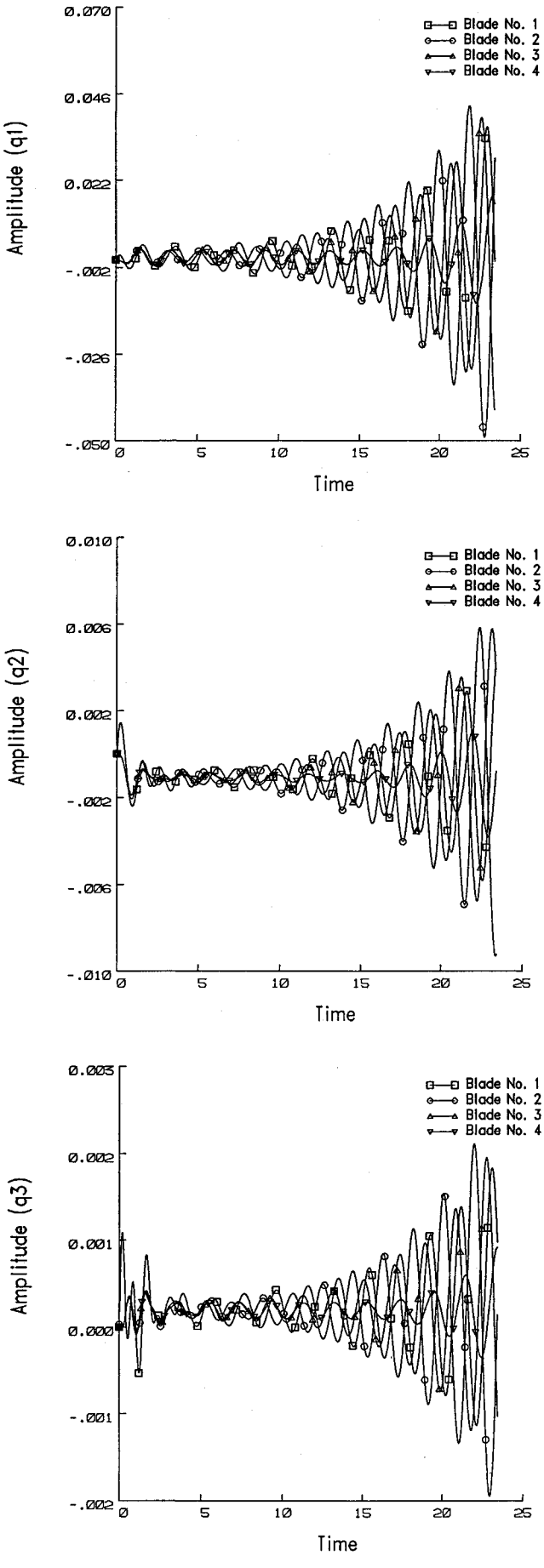

Fig. 6 Response of normal modes for SR3C-X2 with eight blades operating at $M_\infty = 0.7$, $J = 3.55$, and $b = 61.2$ deg.

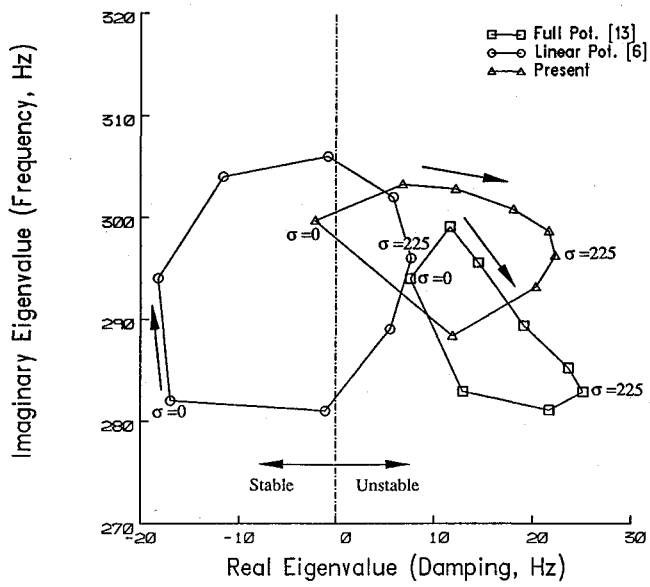

Fig. 7 Eigenvalue plot for SR3C-X2 with eight blades operating at $J = 3.55$ and $b = 61.2$ deg.

the experiment was 274 Hz, whereas, flutter frequency calculated from the frequency domain analysis is 290 Hz. From the time domain analysis, an accurate estimation of frequency is not possible with the length of response signal calculated. The time histories have not yet locked into flutter and the flutter frequency has not yet reached steady state. However, analyzing the calculated time responses, the flutter frequency is obtained between 277 and 285 Hz, depending upon the portion of time response analyzed. This indicates qualitative agreement with the measured flutter frequency. A longer calculated response time should provide a better frequency agreement.

As mentioned earlier, the flutter frequency lies between the first and second blade normal mode frequencies. Since the calculated normal mode frequencies, from the finite element analysis, for the second and third modes are higher than measured, the calculated flutter frequency should also be higher than measured. The frequency correlation can be improved further by improving the blade structural model such that the normal mode frequencies for all of the modes agree well with measured frequencies. Also, the simplifying assumptions made for the analysis of the rotor, such as, no structural coupling and tuned rotor, may contribute to the difference in calculated and measured flutter frequencies.

Eight Blades

The calculations were next carried out for eight blades. For this case the experiment reported the flutter boundary to be at $M_\infty = 0.60$, $J = 3.55$, and 225-deg interblade phase angle.[3] The analysis was carried out for $M_\infty = 0.5$ and 0.7. The time and frequency domain analyses for $M_\infty = 0.5$ had stable response (not shown). The time domain response for $M_\infty = 0.7$ is shown in Fig. 6. Again, only one blade was perturbed. The calculations were carried out until the response for all of the blades started growing. For the sake of clarity, the responses of only four blades are shown, the other blades show a similar response. The frequency domain results are shown in Fig. 7. Also plotted in this figure are the results obtained from the full potential scheme[13] and linear potential scheme (ASTROP3) (Ref. 7). All three analyses captured the correct flutter interblade phase angle mode, but varied in the values of real and imaginary eigenvalues. Of the three responses, the ASTROP3 results are the least conservative, and the full potential are the most conservative.

Comparing Figs. 3 and 6 one can see that the response in Fig. 6 grows more rapidly as compared to Fig. 3. Except for the number of blades in the propfan, all of the other parameters

are the same for these two cases. This implies that the eight-blades case is more unstable than the four blades, indicating that cascading has a destabilizing effect on stability. The frequency domain analysis also shows similar behavior. The aerodynamic damping is much more destabilizing (larger real part of eigenvalue) for the eight blades (Fig. 7) than for the four blades (Fig. 5). A similar observation was also made by Mehmed et al.[2] for another propfan (SR5) in Ref. 2.

All of the previous computations were performed on the Cray Y-MP computer, available at NASA Lewis Research Center. For a grid size of $100 \times 33 \times 21$, used for each block, the total memory and CPU time per time step required were 3.2 MW and 1.7 s, respectively. A typical time domain analysis of a four-bladed rotor required approximately 12 h of CPU time, whereas the frequency domain analysis with three modes included required 15 h of CPU time for the same case.

Concluding Remarks

A three-dimensional Euler aeroelastic solver has been developed and applied to a propfan configuration to analyze classical flutter. An arbitrary number of structural modes and all possible interblade phase angles of a blade row can be analyzed simultaneously, using either the time domain or the frequency domain aeroelastic analysis technique. The analysis was verified using experimental flutter data for an SR3C-X2 propfan at subsonic relative flows. The results obtained compared well for flutter Mach number and interblade phase angle. The results obtained from time and frequency domain analyses correlated well with each other. For this propfan, the flutter occurs in a coupled mode, between the first and second natural modes. Coupled mode flutter requires analyses that include several structural modes. Single mode analysis will not be sufficient in such cases. The analysis also showed strong effects of cascading. For identical flight conditions, rotors with a larger number of blades tended to be more unstable.

The analyses based on Euler equations are computationally expensive, and are not suitable for routine applications, especially for rotors with a large number of blades. Additional capabilities need to be developed to increase the domain of application of the analysis and improve the efficiency. The capability to analyze the problems where the viscosity plays an important role such as stall flutter or instability because of shock and boundary-layer interaction will require methods based on Navier–Stokes equations. For viscous analyses to be practical and affordable, the size of the problem will need to be reduced. Methods that use only the relevant eigenmodes of the system (reduced-order-modeling), or simulation of multiple blade passage analysis using single blade passage (phase-lagged boundary conditions), need to be developed.

Acknowledgments

This work has been carried out under NASA Grant NAG3-1230 from the Structural Dynamics Branch at NASA Lewis Research Center in Cleveland, Ohio. The authors acknowledge M. H. Williams of Purdue University for valuable discussions and suggestions.

References

[1]Mitchell, G. A., and Mikkelson, D. C., "Summary and Recent Results from the NASA Advanced High-Speed Propeller Research Program," AIAA Paper 82-1119, June 1982.

[2]Mehmed, O., Kaza, K. R. V., Lubomski, J. F., and Kielb, R. E., "Bending-Torsion Flutter of a Highly Swept Advanced Turboprop," NASA TM 82975, Oct. 1982.

[3]Mehmed, O., and Kaza, K. R. V., "Experimental Classical Flutter Results of a Composite Advanced Turboprop Model," NASA TM-88792, July 1986.

[4]Elchuri, V., and Smith, G. C. C., "Flutter Analysis of Advanced Turbopropellers," *AIAA Journal*, Vol. 22, No. 6, 1984, pp. 801, 802.

[5]Turnberg, J. E., "Classical Flutter Stability of Swept Propellers," AIAA Paper 83-0847, May 1983.

[6]Williams, M. H., and Hwang, C., "Three Dimensional Unsteady Aerodynamics and Aeroelastic Response of Advanced Turboprops," AIAA Paper 86-0846, May 1986.

[7]Kaza, K. R. V., Mehmed, O., Narayanan, G. V., and Murthy, D. V., "Flutter Investigation of a Composite Propfan Model," *Journal of Aircraft*, Vol. 26, No. 8, 1989, pp. 772–780.

[8]Kaza, K. R. V., "Development of Aeroelastic Analysis Methods for Turborotors and Propfans—Including Mistuning," Vol. 1, NASA CP 3003, May 1988, pp. 247–262.

[9]Verdon, J. M., and Caspar, J. R., "A Linearized Unsteady Aerodynamic Analysis for Transonic Cascades," *Journal of Fluid Mechanics*, Vol. 149, Dec. 1984, pp. 403–429.

[10]Bakhle, M. A., Reddy, T. S. R., and Keith, T. G., Jr., "Time Domain Flutter Analysis of Cascades Using a Full-Potential Solver," *AIAA Journal*, Vol. 30, No. 1, 1992, pp. 163–170.

[11]Huff, D. L., "Numerical Analysis of Flow Through Oscillating Cascade Sections," *Journal of Propulsion and Power*, Vol. 8, No. 4, 1992, pp. 815–822.

[12]Ku, C. C., and Williams, M. H., "Three Dimensional Full Potential Method for the Aeroelastic Modeling of Propfans," AIAA Paper 90-1120, April 1990.

[13]Bakhle, M. A., Keith, T. G., Jr., and Williams, M. H., "Unsteady Aerodynamics and Flutter Based on the Potential Equation," AIAA Paper 93-2086, June 1993.

[14]Srivastava, R., "An Efficient Hybrid Scheme for the Solution of Rotational Flow Around Advanced Propellers," Ph.D. Dissertation, Georgia Inst. of Technology, Atlanta, GA, Aug. 1990.

[15]Srivastava, R., Sankar, N. L., Reddy, T. S. R., and Huff, D. L., "Application of an Efficient Hybrid Scheme for Aeroelastic Analysis of Advanced Propellers," *Journal of Propulsion and Power*, Vol. 7, No. 5, 1991, pp. 767–775.

[16]Beam, R. M., and Warming, R. F., "An Implicit Factored Scheme for the Compressible Navier-Stokes Equations," *AIAA Journal*, Vol. 16, No. 4, 1978, pp. 393–401.

[17]Horlock, J. H., *Axial Flow Turbines—Fluid Mechanics and Thermodynamics*, Krieger, Malabar, FL, 1982, pp. 11–13, 148.

[18]Lane, F., "System Mode Shapes in the Flutter of Compressor Blade Rows," *Journal of the Aeronautical Sciences*, Vol. 23, Jan. 1956, pp. 54–66.